2005-01-2338

Experimental Study of Structure-Borne Noise Transfer Paths over the Mid-Frequency Regime

Seungbo Kim
The Goodyear Tire & Rubber Company

Akira Inoue and Rajendra Singh
Acoustics and Dynamics Laboratory, The Ohio State University

ABSTRACT

This article examines the structure-borne noise transfer path measures by using a laboratory experiment with simulated engine and passenger compartments. It is excited by an emulated powertrain unit that is mounted in the engine room through three hard mounts. Indirect estimation methods for dynamic interfacial forces are first compared with direct measurements over the mid frequency regime. Two alternate path analysis issues, with focus on partial pressures in the receiver room, are then examined. This experimental study clearly demonstrates the strengths and limitations of path rank ordering schemes and analysis methods though only the translational motions are considered.

1. INTRODUCTION

Structure-borne noise in many automotive sub-systems is transmitted through multiple paths and significant dynamic interactions among paths occur; such paths include mounts, suspensions, isolators and structural connections. Proper rank ordering of structural paths is crucial before serious problems related to mounting or suspension systems could be addressed [1, 2]. The role of multiple structural paths is not well documented, although the isolation effects of mounts and isolators have been studied [3-6]. Further, multiple paths and their interactions may exhibit distinct characteristics from a single path system [4, 7, 8]. Direct measurement of the structure-borne noise transmission in such a system is sometimes arduous, and therefore an indirect estimation scheme is needed. Identification of the dominant path(s) in the sub-systems is crucial for subsequent passive control in order to achieve the attenuation levels. Power flow has been used to indicate the vibration transmission efficiency of a few systems [4-9]. However, the power flow through a path in multiple path problem may inherently assume negative values, which would make the analysis troublesome. In this article, we employ an experimental study to address some of the above mentioned problems, by using a simplified automotive system as a source-path-receiver system. Chief objectives of this study are. 1. Develop an experimental procedure for structure-borne noise transfer path measures. 2. Examine the indirect methods to estimate interfacial forces at paths. 3. Investigate the path rank ordering schemes in terms of structure-borne noise transmission. The scope of this study is limited to the frequency domain analysis of a linear time-invariant system, over the mid-frequency regime. Only the translational motions are considered, and thus the multi-dimensional rotational effects would not be included. Scientific issues and results would be only briefly discussed.

2. EXPERIMENTAL SYSTEM AND TYPICAL MEASUREMENTS

Configuration: The experimental system consists of source and receiver chambers. These two chambers simulate the engine and passenger compartments, respectively, as depicted in Figure 1. A motor and an air pump are fixed on a T-shape plate, as shown in Figure 2, which emulate a powertrain unit. Both motor and pump act as the vibration sources, and each source can be operated and controlled separately, and thus they are uncorrelated.

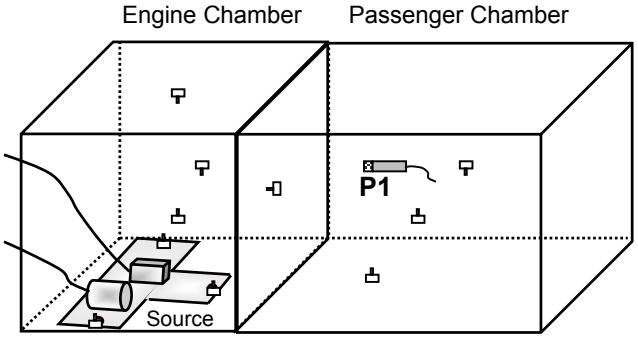

Figure 1. Schematic of the experimental system for simulated vehicle system.

The powertrain unit is mounted on the base of the source chamber by three hard mounts which constitute the main structure-borne transmission paths. We would attempt to quantify these paths in this study.

The structure-borne vibration is transmitted through three paths, then to the base of the source chamber, and finally is transmitted into the receiver chamber as shown in Figure 3. Three microphones are installed in the receiver chamber to measure sound pressures. The source chamber is open at the left side in order to conduct the impact hammer testing (for the acquisition of transfer functions), but the receiver chamber is closed to minimize the air-borne noise paths.

The concept of source-path-receiver is also depicted for this system in Figure 3 where the receiver, that consists of source chamber and receiver chamber, is denoted by dotted lines. Our article focuses on the role of each mount path to sound pressure at a receiver location, and thus the structure-borne noise paths imply the mount paths in this paper. Further, throughout this paper, the path input points are referred to as the driving points which are at the base of the source chamber as we primarily deal with the path variables at these interfaces.

The motor and air pump are operated at 6 different speed levels, including the zero speed. Therefore, the two-source unit has 36 discrete speed combinations. Accelerometers, microphones and impedance heads are used in both chambers. Refer to Table 1 for a list of instrumentation used for this experiment.

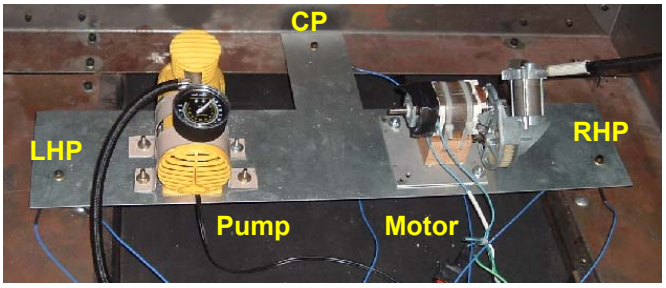

Figure 2. Emulated powertrain unit that consists of an air pump, a motor and a T-shaped base plate.

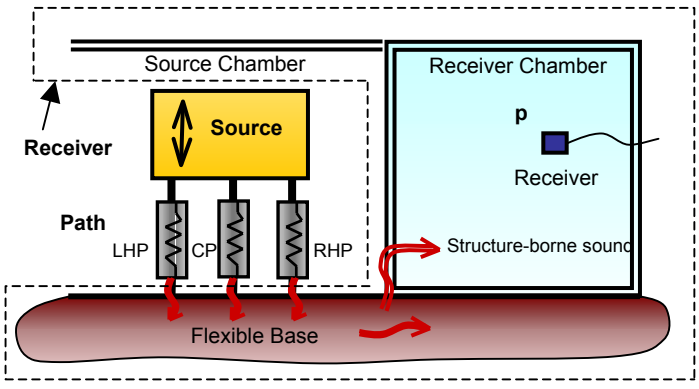

Figure 3. Structure-borne noise transmission paths of the experimental system. Left, center and right paths are connected to the source chamber structure via hard mounts and are denoted here as LHP, CP and RHP respectively.

Table 1. Instruments used for the transfer path experiments.

	Source Chamber	Receiver Chamber
Accelerometers	48	3
Microphones	-	3
Impedance Heads	3	-
Impact Hammer	1	-
Channels per Acquisition	15	
Power Amplifiers	2	

Measurement Procedures: Accelerations are measured at 48 points in the source chamber to estimate the forces through the paths. The source chamber has 5 surfaces since the left side is open. Nine accelerometers are installed on each surface except the bottom surface, which has 3 more locations on the path mounting points. The maximum number of channels for each measurement is 15, but the operational structural responses at the LHP are synchronized for alternate acquisition record sets. Thus consistent phase relations are maintained for the entire measurement sets. Note that vibrations are generated by uncorrelated pump and motor only: no shakers or impact hammers are applied to the source unit when the sources are running. Thus one reference is sufficient for synchronizing operating structural and acoustic responses at mounts and receiver locations. Although 3 microphones are used to measure the sound pressures, only one microphone (at P1 as shown in Figure 1) is utilized in the analysis reported in this article. The impedance heads measure path forces and accelerations in only one translational direction. Motions in other directions are not considered here.

First, the impact testing is conducted to obtain the transfer functions of the two-chamber system. For this process, the powertrain unit is disconnected from the source room structure and an impulsive force is applied to each path mounting point. The accelerometers and the microphones measure the following frequency responses on a narrow band basis from 100 to 2800 Hz: a/F (m/s^{2}N) and p/F (Pa/N). Second, the motor and the air pump are operated after the powertrain unit is installed. The impedance heads, as well as the accelerometers and the microphones, measure the operational responses at the same locations. Such direct measurements will be compared with the indirect estimations. Finally, by using the above mentioned measured data, paths are rank ordered by the indirect force estimation methods, power flow spectral estimations, and weighted mean-square force and velocity calculations. Typical measured spectra are shown in terms of structural and acoustic frequency response functions and sound pressures in Figures 4 and 5 when the source excitations are set at the highest level (say 5, Pump at 10V and Motor at 60V) and at 36 discrete speed levels respectively. Only the analyses when the sources are run at the highest levels are presented in the subsequent sections of this paper.

3. INDIRECT METHODS OF ESTIMATING PATH FORCES

Practical difficulties would exist in directly measuring the interfacial path forces in typical automotive systems. Consequently, the path forces would need to be estimated via an indirect method. Here, two alternate indirect methods are employed to estimate the interfacial path forces. The operating structural velocity response vector (V) at frequency ω is expressed as follows where $[\mathbf{V}/\mathbf{F}]$ is the mobility matrix and $\mathbf{F}$ is the interfacial force vector. Here, subscript ℓ and *n* are the number of response and path locations, respectively.

$$[\mathbf{V}]_{l\times 1} = \left[\frac{\mathbf{V}}{\mathbf{F}}\right]_{l\times n} \cdot [\mathbf{F}]_{n\times 1} . \tag{1}$$

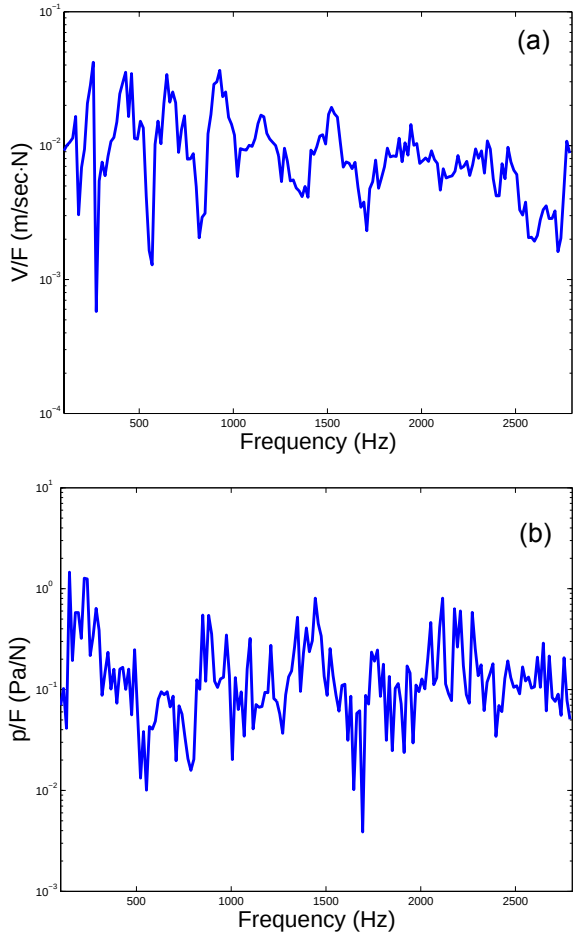

Figure 4. Measured acoustic and structural frequency response functions: (a) driving point mobility at the left path; (b) acoustic FRF (p/F) with sound pressure in the receiver room and force at the center path.

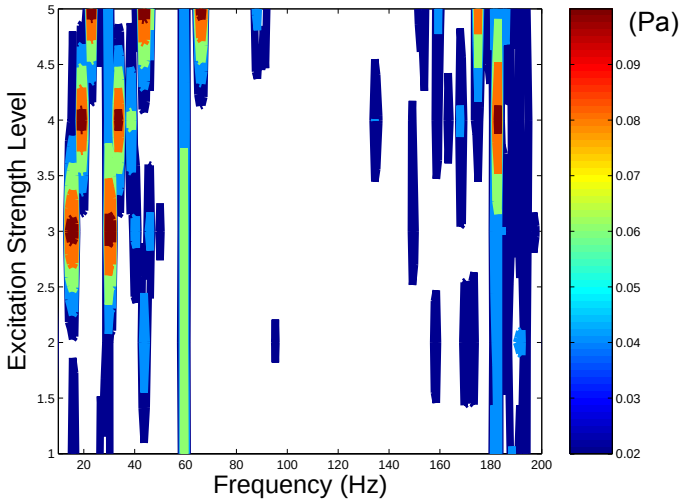

Figure 5. Sound pressure map measured at P1 in the receiver room with 5 excitation levels up to 200 Hz. Area in white is less than 0.02 Pa (rms).

Impedance Method: First, only the responses at the driving ends of paths are considered. In such case, interfacial forces at any frequency are estimated as follows where $\mathbf{Z}$ is the driving point impedance matrix of all paths combined.

$$[\mathbf{F}]_{n\times 1} = [\mathbf{Z}]_{n\times n} \cdot [\mathbf{V}]_{n\times 1} = \left[\frac{\mathbf{V}}{\mathbf{F}}\right]^{-1}_{n\times n} \cdot [\mathbf{V}]_{n\times 1} . \tag{2}$$

In this article, this force estimation method is referred to as the impedance method. Further, $\mathbf{Z}$ is obtained via the measured driving point mobility matrix since the blocked boundary conditions, that are associated with the impedance matrix, are often impractical to implement in many cases. Thus, $\mathbf{Z} = [\mathbf{V}/\mathbf{F}]^{-1}$.

Least-Squares Method: Next, the operating responses and mobilities at ℓ number of locations are considered along with the driving ends at paths. From Equation (1), the interfacial force vector is estimated as follows where the superscript + implies a pseudo inverse.

$$[\mathbf{F}]_{n\times 1} = \left[\frac{\mathbf{V}}{\mathbf{F}}\right]^{+}_{l\times n} \cdot [\mathbf{V}]_{l\times 1} , \tag{3}$$

$$\left[\frac{\mathbf{V}}{\mathbf{F}}\right]^{+}_{l\times n} = \left[\left[\frac{\mathbf{V}}{\mathbf{F}}\right]^{T}\left[\frac{\mathbf{V}}{\mathbf{F}}\right]\right]^{-1} \cdot \left[\frac{\mathbf{V}}{\mathbf{F}}\right]^{T} . \tag{4}$$

In this article, this force estimation approach is referred to as the least-square method. Further, the mobility matrix $[\mathbf{V}/\mathbf{F}] = [\mathbf{V}/\mathbf{F}]_{48\times 3}$ is measured at 48 points in the source chamber including the path mounting point mobility matrix $[\mathbf{V}/\mathbf{F}]_{3\times 3}$. All spectra are obtained in narrow band from 100 to 2800 Hz and then converted to the one-third octave band spectra.

Estimated Force Results: The interfacial force spectra are estimated for three paths by using the above two methods. Estimations are shown in **Figure 6** and compared with the direct force measurements. **Figure 6** shows that the impedance method yields a better estimation of the measured forces over a wide range of

frequencies. However, the force estimated via the impedance method (at the center path) deviates from the measured one up to around 500 Hz, as shown in **Figure 6**(b). It is also observed in **Figure 6** that estimated forces with the least-squares method produce more deviations than the ones with the impedance method and those discrepancies are more pronounced for left and right paths.

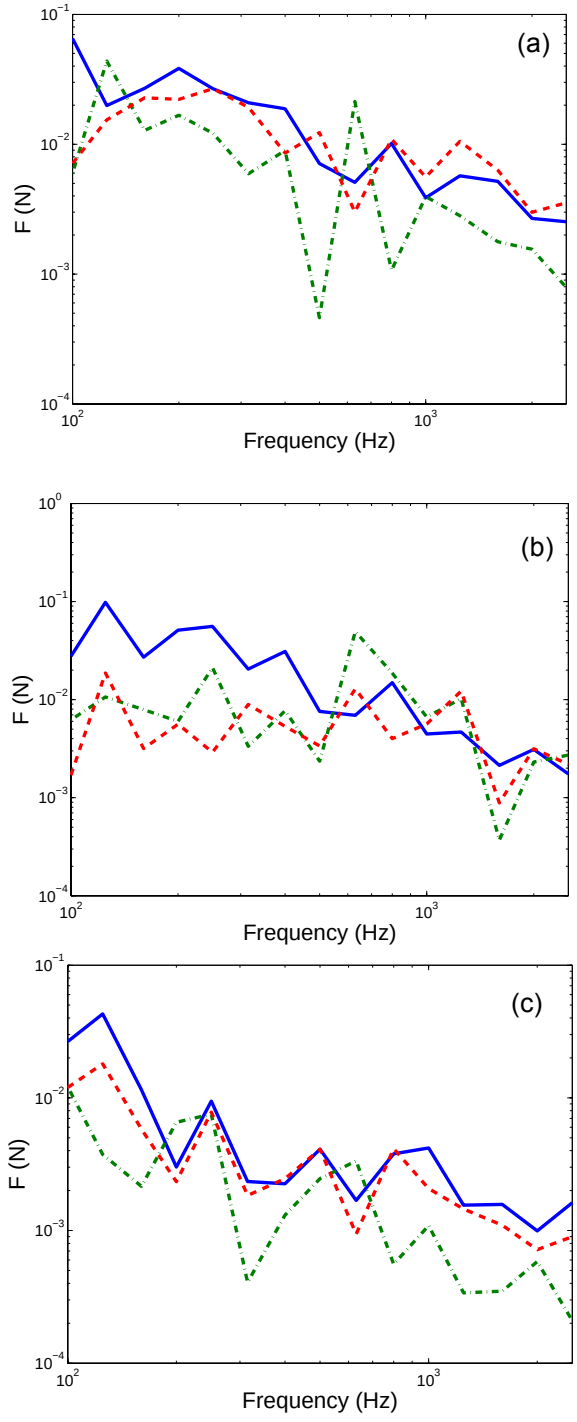

Figure 6. Estimated path forces and comparisons with direct measurements: (a) left path; (b) center path; (c) right path. Key: ——, measured force; — · — ·, estimated force via the least square method; — — —, estimated force via the impedance method.

4. PATH RANK ORDERS BASED ON PARTIAL SOUND PRESURES

Partial Pressure Formulations: Four alternate schemes are employed to rank order the structural paths in terms of the partial sound pressure components. First, consider the mobility and impedance formulations, which represent free and blocked boundary conditions respectively. Each is evaluated in terms of forces or velocities. The four formulations are written as follows where p is the sound pressure in the receiver room at a given frequency and subscripts M, Z, F and V represent mobility formulation, impedance formulation, measured force and measured velocity respectively:

$$p_{FM}(\omega) = \left[\frac{\mathbf{p}}{\mathbf{F}}\right]_{1\times 3}\left[\mathbf{F_m}\right]_{3\times 1} = \sum_i \left[p_{FM,i}\right] = \sum_i \left[\frac{p}{F_i}\right] F_{mi}\,, \quad (5)$$

$$p_{FZ}(\omega) = \left[\frac{\mathbf{p}}{\mathbf{V}}\right]_{1\times 3}\left[\mathbf{V_e}\right]_{3\times 1} = \sum_i \left[p_{FZ,i}\right] = \sum_i \left[\frac{p}{V_i}\right] V_{ei}\,, \quad (6)$$

$$p_{VM}(\omega) = \left[\frac{\mathbf{p}}{\mathbf{F}}\right]_{1\times 3}\left[\mathbf{F_e}\right]_{3\times 1} = \sum_i \left[p_{VM,i}\right] = \sum_i \left[\frac{p}{F_i}\right] F_{ei}\,, \quad (7)$$

$$p_{VZ}(\omega) = \left[\frac{\mathbf{p}}{\mathbf{V}}\right]_{1\times 3}\left[\mathbf{V_m}\right]_{3\times 1} = \sum_i \left[p_{VZ,i}\right] = \sum_i \left[\frac{p}{V_i}\right] V_{mi}\,. \quad (8)$$

Here, subscripts m and e denote measured and estimated quantities respectively, and subscript i indicates the path component of interest. For example, $[\mathbf{F}_m]$, $[\mathbf{V}_m]$ and $\left[\frac{\mathbf{P}}{\mathbf{F}}\right]$ are the measured force, velocity and acoustic transfer function respectively. Further, $[\mathbf{p}/\mathbf{V}]_{1\times 3}$ and $[\mathbf{V}_e]_{3\times 1}$ are estimated as follows by using the above measured quantities along with measured $[\mathbf{p}/\mathbf{F}]_{1\times 3}$ mobility matrix $[\mathbf{M}]$:

$$\left[\frac{\mathbf{p}}{\mathbf{V}}\right]_{1\times 3} = \left[\frac{\mathbf{p}}{\mathbf{F}}\right]_{1\times 3}\left[\mathbf{M}\right]^{-1}_{3\times 3}\,,\ \left[\mathbf{V_e}\right]_{3\times 1} = \left[\mathbf{M}\right]_{3\times 3}\left[\mathbf{F_m}\right]_{3\times 1}\,. \quad (9a, b)$$

Furthermore, $[\mathbf{F}_e]$ is estimated by using (2). Note that $p_{FM}(\omega) = p_{FZ}(\omega)$ and $p_{VM}(\omega) = p_{VZ}(\omega)$ although their partial components are not necessarily the same such as $p_{FM,i} \neq p_{FZ,i}$ and so on. Sound pressures in the receiver room are estimated in Figure 7 via measured force and velocity formulations of Equations (5) to (8). These estimations are compared with the direct measurements of sound pressures. Overall, the estimated sound pressures match well the measured ones over a broad range of frequencies. However, the sound pressure that is estimated via the measured force shows a relatively large deviation from the direct measurements up to 300 Hz.

Rank Orders Based on Force or Velocity Spectra: Rank orders of paths based on measured forces and velocities are shown in Figure 8. Measured force spectra show that right path is the weakest and left and center paths

are equally dominant, as shown in Figure 8(a). Unlike the order based on forces, the order of dominance is clear in the velocity spectra over a broad range of frequencies. Figure 8(b) shows that velocity is maximum at the left path and the center path is the weakest.

A spectral average of the path forces is calculated, between 100 and 2800 Hz, and these results are shown in Table 2. The average over the mid-frequency regime shows that the center path is the most dominant of the three in terms of the transmitted force. On the other hand, the right and left paths seem to transmit equal forces to the base.

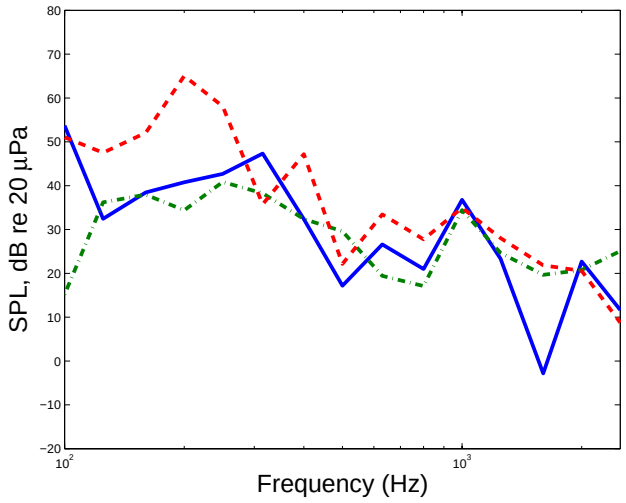

Figure 7. Estimated sound pressure (SPL) in the receiver room. Key: ——, measured SPL; — · — · —, estimated SPL ($p_{FM} = p_{FZ}$) using measured velocity; — — —, estimated SPL ($p_{VM} = p_{VZ}$) using measured force.

Rank Orders Using Measured Path Forces: **Figure 9 shows the partial sound pressure spectra that** are estimated by the mobility method based on the measured path forces. Overall, the center path is dominant in the partial sound pressure spectra as shown in Figure 9.

Table 2. Spectral averages (100 – 2800 Hz) of measured forces and velocities at paths.

Path measure	Left Path	Center Path	Right Path
Force	7,982 µN	25,657 µN	7,996 µN
Velocity	67.08 µm/s	37.47 µm/s	73.82 µm/s

In order to compare the partial sound pressures based on the impedance and mobility formulations, the following relative sound pressure level (Δp) is defined (in dB) where subscripts *i* and *j* are path indices.

$$\Delta p_{i-j} = 20\log_{10}\left(\frac{|p_i|}{|p_j|}\right), \qquad i, j = 1, 2, 3. \qquad (10)$$

Results are shown in Figure 10. Relative sound pressure levels of Figure 10 show that the rank order of paths and their relative strengths are formulation-dependent. For example, the right path is dominant in the impedance method around 700 Hz but the partial sound pressure of the left path is larger than the one of right path in the mobility representation at that frequency, as shown in Figure 10(c). However, note that total sound pressures of Figure 10 from either the mobility or impedance methods should be identical.

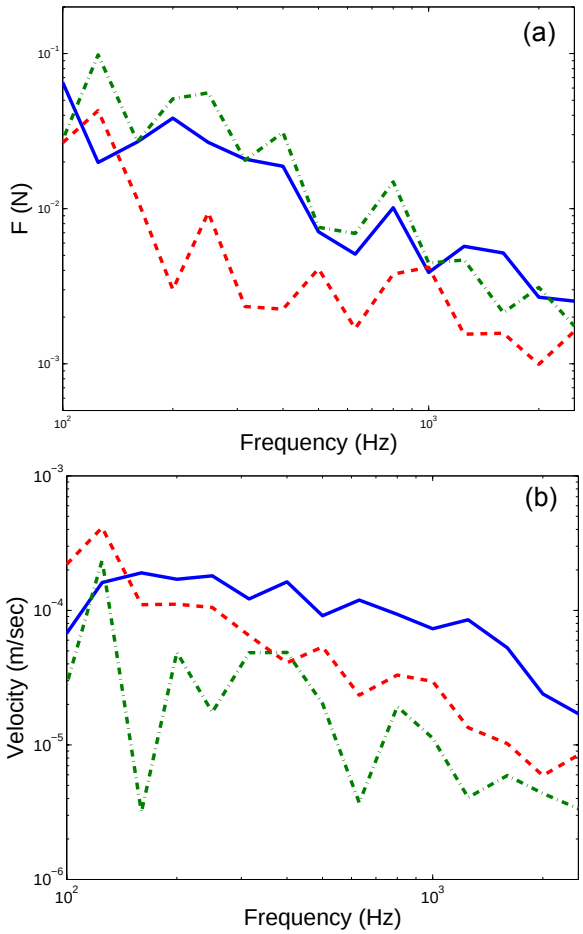

Figure 8. Measured force (a) and velocity (b) at paths. Key: ——, left path; — · — · —, center path; — — —, right path.

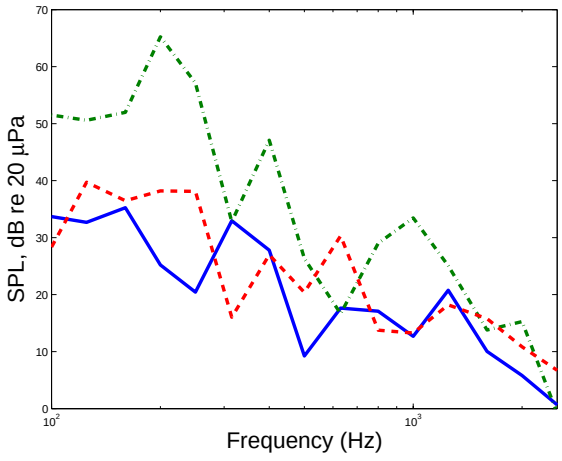

Figure 9. Estimated partial sound pressures via the mobility method with measured forces by using (5). Key: ——, left path; — · — · —, center path; — — —, right path.

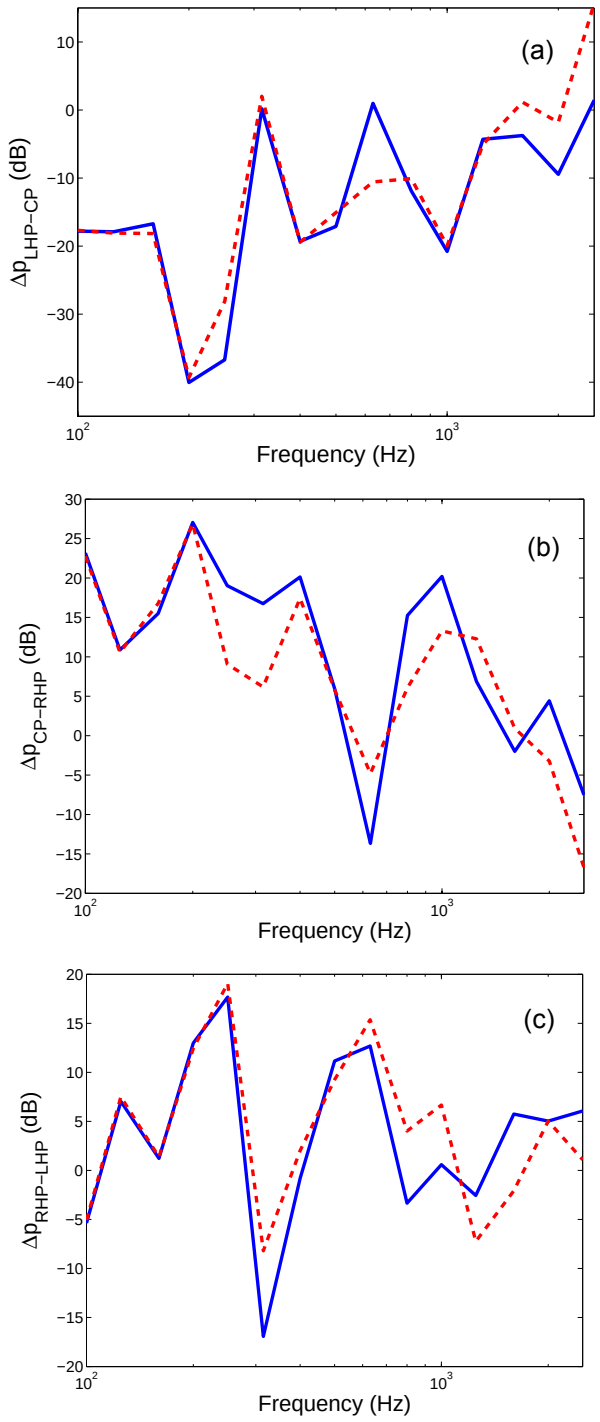

Figure 10. Relative partial sound pressures: (a) Δp_{LHP-CP}; (b) Δp_{CP-RHP}; (c) $\Delta p_{RHP-LHP}$. Key: ——, mobility method; – – –, impedance method.

Vectorial Representation of Paths: Sound pressure components are next represented in a vectorial form in Figure 11 for both mobility and impedance formulations. Figure 11 illustrates that the sound pressure components from the three paths constitute the total (measured) sound pressure in different ways for the mobility and impedance methods. Hence, Figure 11 further reveals that the descriptions of path contributions to the resulting partial pressures depend on the boundary condition formulation, such as the blocked and free conditions that are shown in Figure 11(a) and (b) respectively. Furthermore, there may be an infinite number of vectorial representations to describe the same sound pressure spectra at an observation point in the passenger cabin. Nonetheless, it appears that the mobility type formulation is preferred in practice since the free boundary conditions are easily implemented. Further note that total sound pressure is the same (as it should be) for those alternate representations; see the solid lines in Figures 11(a) and (b).

Rank Order with Measured Path Forces: Partial sound pressures that are estimated with the measured velocities are shown in Figure 12. Unlike the ones with measured forces of Figure 9, the center path is not as dominant. And, the right and center paths are somewhat the same up to 300 Hz, as shown in Figure 12.

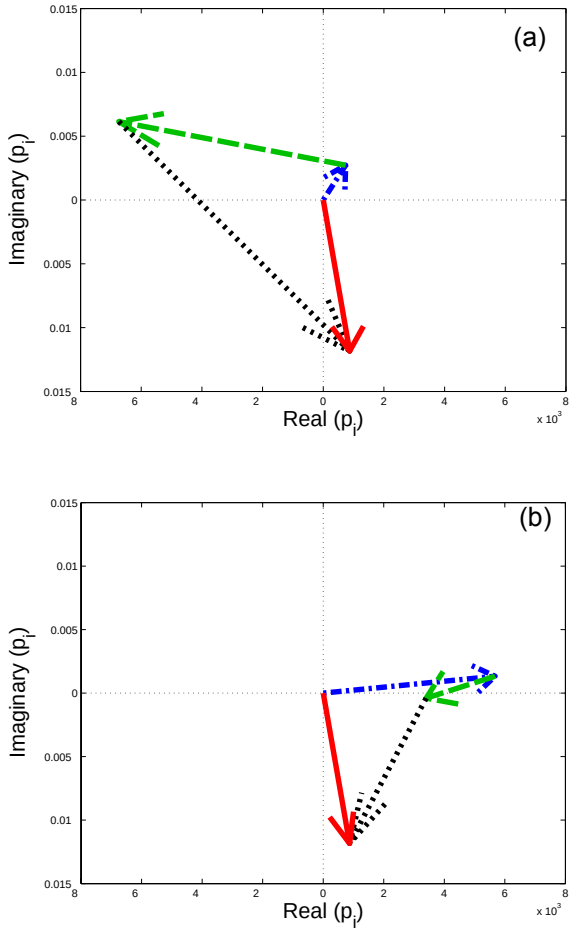

Figure 11. Vectorial representations of the partial sound pressures at 227 Hz based on measured forces: (a) impedance method; (b) mobility method. Key: ——, total sound pressure, – – –, from left path; – · –, from center path; ▪▪▪▪▪▪▪▪▪, from right path.

The spectral averages are tabulated in Table 3. The center path is the most dominant in both estimation methods, though the rank order of the left (or the right) path depends on the method. This spectral average is taken in the mid-frequency regime since it more clearly suggests the rank order of each path.

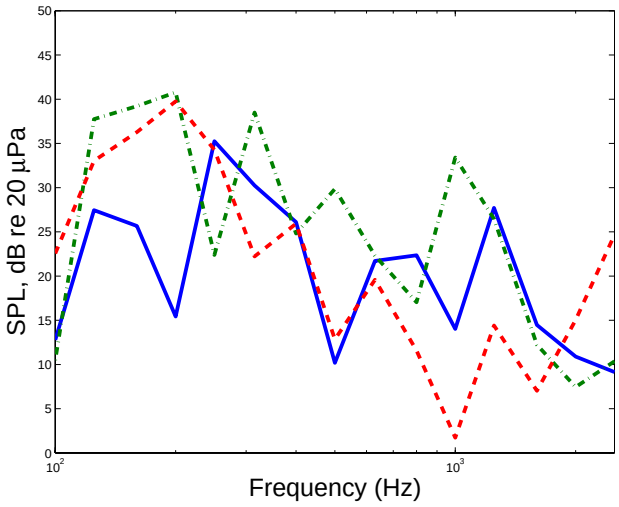

Figure 12. Path rank order of partial sound pressure via Mobility method with measured velocities by using (7). Key: ——, left path; — · — ·, center path; — — —, right path.

Table 3. Spectral averages (100 – 2800 Hz) of partial sound pressures (μPa) as estimated by the impedance and mobility methods.

(μPa)	Left Path	Center Path	Right Path
Impedance Method	1718	2207	1943
Mobility Method	1103	4056	1033

Although the total estimated sound pressures show somewhat lower spectral magnitudes over the lower frequency regime, the estimated partial sound pressure may be used as a path rank quantifier as that would suggest a distinct contribution to the total sound pressure. Even though the precise role of the structure-borne noise through each path to the sound pressure (at a receiver point) is still not clearly understood, our proposed estimation methods (based on the impedance and mobility formulations) should give lead to further studies.

5. PATH RANK ORDERS BASED ON ENERGY QUANTIFIERS

The spectral vibration power (Π), as defined below, is employed to rank order paths.

$$\Pi_{IN}(\omega) = \frac{\omega}{2\pi}\int_0^{2\pi/\omega} F(t)V(t)\,dt = \frac{1}{2}|F||V|\cos\phi = \frac{1}{2}Re[\tilde{F}(\omega)\tilde{V}^*(\omega)] = \frac{1}{2}Re[\tilde{V}(\omega)\tilde{F}^*(\omega)] \quad (11)$$

Note that the vibration power per cycle represents dissipated energy of a harmonic system. Refer to our articles for further details [4, 11]. Unlike the force or velocity vectors, the units of Π (a scalar quantity) are compatible for rotational and translational directions. Therefore, the power flow could be easily used. Refer to [4] for an explanation. Further, our earlier work shows a close correlation between sound radiation from a 'L' structure receiver to the free field and the vibration power at receiver driving points [4]. Vibration powers for three paths are obtained by using measured forces and velocities of Figure 8. Results are shown in Figure 13(a) and (b) for total power and power components respectively.

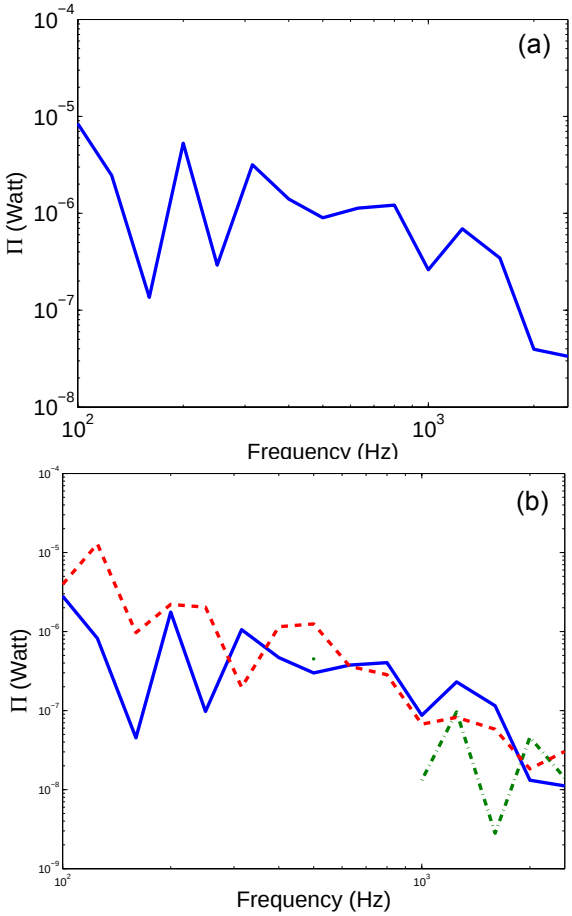

Figure 13. Power flow (W) through paths: (a) total power flow; (b) power flow through each path. Key: (a) ——, total power flow; (b) ——, from left path; — · — ·, from center path; — — —, from right path. Negative values are not shown here.

The power components of Figure 13(b) show that the right path is more dominant from 100 to 300 Hz. Further, Figure 13(b) shows that Π at the center path exhibits negative values over a wide range of frequencies, say from 100 to 1000 Hz. Note that the power flow through any path may be negative for multiple paths case. Negative power flow may imply the power flow in a reverse manner, say from receiver to source unit in this case. Refer to our earlier article for an example of such reverse power flow [4]. (Further, consider an analytical uni-axial structure that is applied by two separate excitations at both ends. No coupling in the system or no physical connection between the two independent excitations exists. The vibration power at either end may become negative although there is no system for energy dissipation beyond the end points). Nonetheless, an interpretation of the negative power flow is somewhat cumbersome. The total power should

be positive at all frequencies as shown in Figure 13 (a). Caution must be however exercised since the total power could be negative for an experimental system especially when some degrees of freedom (say the rotational directions) are not taken into account. Refer to [4] for an explanation. Next, define the mean-square force (Ψ_F^2) and velocity (Ψ_V^2) for uni-directional motions as:

$$\Psi_{F,i}^2 = < F_i^2(t) >_t = \frac{\omega}{2\pi}\int_0^{2\pi/\omega} F_i^2(t)\,dt = \frac{1}{2}Re[\tilde{F}_i\tilde{F}_i^*] = \frac{|F_i|^2}{2} \qquad (12a)$$

$$\Psi_{V,i}^2 = < V_i^2(t) >_t = \frac{\omega}{2\pi}\int_0^{2\pi/\omega} V_i^2(t)\,dt = \frac{1}{2}Re[\tilde{V}_i\tilde{V}_i^*] = \frac{|V_i|^2}{2} \qquad (12b)$$

The $\Psi_{F,i}^2$ and $\Psi_{V,i}^2$ are meaningful for uni-directional motions but their relative comparisons are inappropriate for multi-dimensional motions since the units of Ψ^2 terms are not compatible between translational and rotational directions. Therefore, the weighted mean-square quantity Ψ_W^2 that can hold equivalent units for dissimilar motions is employed here to rank order paths along with the driving point mobility M (or its reciprocal that is the impedance Z), corresponding to force (or velocity) variable, as a weighting factor. The weighted mean-square force (Ψ_{WF}^2) and velocity (Ψ_{WV}^2) are defined as

$$\Psi_{WF,i}^2 = \frac{1}{2}Re[\tilde{F}_i\tilde{F}_i^* M_{ii}] = \frac{|F_i|^2}{2}Re[M_{ii}] \qquad (13a)$$

$$\Psi_{WV,i}^2 = \frac{1}{2}Re[\tilde{V}_i\tilde{V}_i^* Z_{ii}] = \frac{|V_i|^2}{2}Re[Z_{ii}] \qquad (13b)$$

The $\Psi_{WF,i}^2$ and $\Psi_{WV,i}^2$ have the units of power and are therefore always positive for a linear system since the real parts of driving point mobility and impedance are positive. Note here that M_{ii} and Z_{ii} are the driving point mobilities and impedances respectively at mount attachment locations of the receiver structure only that is disconnected from paths and source unit. Further, the $\Psi_{WF,i}^2$ (or $\Psi_{WV,i}^2$) represents the power term consisting of force (or moment) and velocity that are induced by the corresponding force (or moment) and velocity in that direction. However, note that $\Psi_{WF,i}^2$ and $\Psi_{WV,i}^2$ do not include the coupling terms unlike the power expression of (11): refer to [4] for more details. The $\Psi_{WF,i}^2$ and $\Psi_{WV,i}^2$ are obtained by using measured velocities and the driving point mobilities for the system; these are shown in Figure 14 and Figure 15 respectively. Figure 14 shows that the center path is dominant at all frequencies except around 650 Hz, and the left and right paths compete with each other depending on frequencies. The dominance of center path is however not observed in Figure 15. For example, the right path is dominant around 100 Hz but the center path dominates around 400Hz for the case. Further, negative values of both and are found over some frequency ranges such as around 200 Hz at the right path. This implies that the actual system may have deviated from the linear system assumption over those frequency regimes.

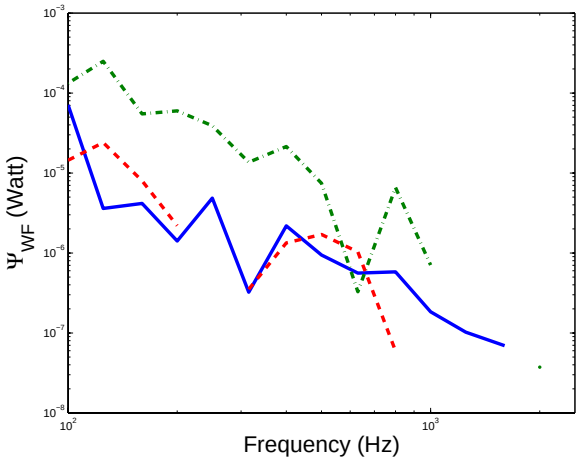

Figure 14. Weighted mean-square path force (Ψ_{WF}^2) components for the system of Figure 1. Key: ——, from left path; — · — ·, from center path; – – –, from right path. Negative values are not shown here.

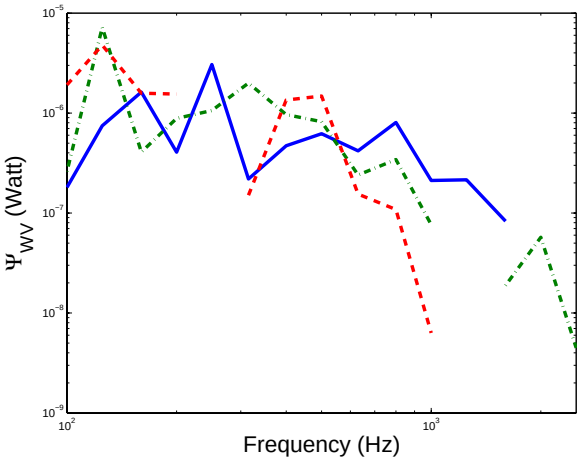

Figure 15. Weighted mean-square velocity (Ψ_{WV}^2) components at the three paths of Figure 1. Key: ——, from left path; — · — ·, from center path; – – –, from right path. Negative values are not shown here.

6. CONCLUSION

Structure-borne noise path measures are experimentally examined using a simulated vehicle system from 100 to 2800 Hz. The experimental system consists of two chambers and an emulated powertrain unit that is installed in the source room via three hard mounts. Acoustic and structural frequency response functions are obtained at a number of locations and then operating responses are measured for various combinations of emulated powertrain speeds. Only the translational motions in the axial direction of mounts are considered here.

First, interfacial path forces are estimated via indirect methods and are compared with the direct measurements. Results show that the impedance

method yields a closer force estimate than the least-squares method.

Second, the paths are rank ordered in terms of the partial sound pressure components at a point in the receiver room. Four alternate rank order schemes are employed to assess the structural noise paths. These schemes include mobility and impedance formulations with either measured path forces or velocities. The center path is dominant over a broad frequency range when the measured force is used along with the mobility formulation but its dominance is not as clear when the measured velocity is used with the same formulation. Further, the path rank order changes when the impedance formulation is employed (depending upon frequencies) although the total sound pressures (as they should) remain the same.

Third, the energy-based measures are employed to assess the noise paths and the spectral powers show that right mount is dominant up to 400 Hz; this result deviates from the rank order found from the partial sound pressure method. However, the negative values of measured powers are observed over a wide range of frequencies and therefore interpretations of the power quantities are not clear. Finally, alternate energy quantities, which are the weighted mean-square force and velocity, are analyzed. The weighted mean-square force shows that the center path is dominant like the partial sound pressure method. But the path rank order is not as clear in the weighted mean-square velocity calculations. Similar to the power case, negative values exist over some frequency bands in the weighted mean-square quantities.

Overall, the rank order calculations by the partial sound pressures or weighted mean square quantities are found to be formulation-sensitive. The vibration power should produce a consistent rank order regardless of the formulation but it involves negative values which require proper interpretation. Such unresolved issues need to be addressed in future along with an examination of other estimation methods and path rank ordering schemes.

Given the complexity of issues, only a summary of the methods and results has been presented though much work has been done [12]. Future research should also consider the rotational degrees of freedom and their effect on rank orders and power values (positive or negative).

ACKNOWLEDGMENTS

The Center for Automotive Research Industrial Consortium at The Ohio State University is gratefully acknowledged for supporting this research since Oct. 2001.

REFERENCES

1. L. CREMER and M. HECKLE 1973 *New York: Springer-Verlag.* Structure-Borne Sound: Structural Vibrations and Sound Radiation at Audio Frequencies.
2. M. A. BERANEK 1988 *Noise and Vibration Control*. Washington, DC: Institute of Noise Control Engineering.
3. S. KIM and R. SINGH 2001 *Journal of Sound and Vibration*, 245(5), 877-913. Multi-Dimensional Characterization of Vibration Isolators over a Wide Range of Frequencies.
4. R. SINGH and S. KIM 2003 *Journal of Sound and Vibration*, 262(3), 419-455. Examination of Multi-Dimensional Vibration Isolation Measures and Their Correlation to Sound Radiation over a Broad Frequency Range.
5. S. KIM and R. SINGH 2003 *SAE paper*, 2003-01-1477. Examination of Some Vibration Isolator Models and Their Effects on Vibration and Structure-borne Noise Transmission
6. M. A. SANDERSON 1996 *Journal of Sound and Vibration*, 198(2), 171-191. Vibration Isolation: Moments and Rotations Included.
7. P. GARDONIO, S. J. ELLIOTT and R. J. PINNINGTON 1997 *Journal of Sound and Vibration*, 207(1), 61-93. Active Isolation of Structural Vibration on a Multiple-Degree-of-Freedom System, Part I: The Dynamics of the System.
8. B. A. T. PETERSON and B. M. GIBBS 1993 *Journal of Sound and Vibration*, 168(1), 157-176. Use of the Source Descriptor Concept in Studies of Multi-Point and Multi-Directional Vibrational Sources.
9. S. KIM and R. SINGH 2003 *SAE paper*, 2003-01-1450. Structure-Borne Noise Measures and Their Correlation to Sound Radiation over a Broad Range of Frequencies
10. P. GARDONIO and M. J. BRENNAN 2002 *Journal of Sound and Vibration*, 249(3), 557-573. On the Origins and Development of Mobility and Impedance Methods in Structural Dynamics.
11. S. KIM and R. SINGH 2004 *Submitted to Journal of Sound and Vibration*, Alternate Methods for Characterizing Spectral Energy Inputs Based Only on Driving Point Mobilities or Impedances.
12. R. Singh, S. Kim, A. Akira, 2001-05, Progress on the Multiple Structure-borne Noise Paths Project, submitted to the members of the CAR Industrial Consortium.

LIST OF SYMBOLS

a	acceleration (m/s^2)
F	force (N)
Δp	relative sound pressure level
i	$\sqrt{-1}$
V	velocity (m/s)
p	sound pressure (Pa)
T	period (seconds)
t	time (seconds)
μ	micro (10^{-6})
Π	time-averaged power (Watt)

ω	frequency (rad/sec)

Superscripts

+	pseudo-inverse
*	complex conjugate
~	complex valued
T	transpose

Subscripts

C	center path
e	estimated
F	measured force
L	left path
R	right path
P1	receiver point P1
i	path index
j	path index
m	measured
n	index
V	measured velocity

Operators

$\mathrm{Im}[\ ]$	Imaginary part
$\mathrm{Re}[\ ]$	real part
$[\ ]_{i\times j}$	(*i* by *j*) matrix, bold type
$\underline{\ }$	vector, bold type

Abbreviations

CP	center path
LHP	left hand side path
RHP	right hand side path

CONTACT

Professor Rajendra Singh
Acoustics and Dynamics Laboratory
Center for Automotive Research
The Ohio State University
Email: singh.3@osu.edu
Phone: 614-292-9044
Website: www.AutoNVH.org